Proceedings of 2021 International Conference on Advanced Robotics and Intelligent Systems
Taipei Nangang Exhibition Center, Taipei, Taiwan, 17-20 August, 2021

# Formation Control Using Output Recurrent Fuzzy Broad Learning System and Incremental Hierarchical Sliding Mode Control for Multiple Ball-Riding Robots with Uncertainties

**Pai-Yu Ou yang, Feng-Chun Tai, and Ching-Chih Tsai**
*Department of Electrical Engineering, National Chung Hsing University, Taichung, Taiwan, ROC*

***Abstract*—This paper presents a cooperative formation control using output recurrent fuzzy broad learning system (ORFBLS) and incremental hierarchical sliding-mode control (IHSMC) for multiple gyro-stabilized inverse-Atlas ball-riding robots (IASBRRs) with uncertainties. The whole multi-IASBRRs system is modeled by a directed and connected graph. This formation controller, simply called ORFBLS-IHSMFC, is proposed to accomplish robust self-balancing and formation control of the IASBRRs in the presence of unknown frictions, mass variations and model uncertainties. The proposed ORFBLS-IHSMFC control law is proven asymptotically stable using Lyapunov stability theory. The obstacle avoidance adopts the well-known potential field method to instantly avoid any static and/or moving obstacles by modifying the current trajectory of each robot and then tracking it. Two simulations are conducted to show the effectiveness and merits of the proposed ORFBLS-IHSMFC with the obstacle avoidance method. The results show that the proposed ORFBLS-IHSMFC is superior to two existing methods, ORBLS- BSMFC and BLS-BSMFC, and the proposed ORFBLS-IHSMFC together with the obstacle avoidance method is shown effective in formation control.**

**Keyword:** *Ball-riding robot, incremental hierarchical sliding-mode control, cooperative formation control, output recurrent fuzzy broad-learning-system (ORFBLS), obstacle avoidance.*

## I. INTRODUCTION

In recent years, the problem of controlling formations of unmanned vehicles has attracted a lot of attention. This work has typically focused on formation keeping or coordination along preplanned trajectories. With more and more cooperation, the proportion of unknown obstacles in the robot's surroundings continues to increase, so avoiding obstacles is essential [1-3].

Neural networks and deep learning algorithms are one of the hottest topics in recent years. With the demands for performance, tens or even hundreds of layers of deep networks have become increasingly important in many science and engineering applications. Such applications is companied with a huge amount of calculations. So without losing of much accuracy done by deep learning approaches, a new broad learning system (BLS) with less computational complexity was proposed by Chen and his research group [4-5]. BLS is indeed a two-layer plat and feedforward neural network for which the first layer is with several mapped feature nodes, the second layer is with many enhancement nodes, and all the outputs of the nodes in both layers are connected to the final output. Recently, a new kind of recurrent BLS (RBLS) was also proposed to carry out time series prediction [6]. Along the trend of the recurrent FBLS, an output RFBLS (ORFBLS) would be developed by feeding the output(s) into enhancement nodes, in order to strength its nonlinear time-varying learning capabilities.

On the other hand, due to benefits from mobile computing and IoT technology, all kinds of self-balancing mobile platforms have been extensively improved. The study in [3] considered the dynamic unicycle to formation control and obstacle avoidance. A type of ball-riding robot has also received extensive attention in the control and automation communities. Among many developed ball-riding robots, there are two types of prototypes with better motion performance. One is the inverse mouse-type mobile platform robot driven by vertical two-dimensional motors, simply called “ballbot”, which was developed by Hollis and his team [7-10]. The other is the inverse-Atlas ball-riding robot driven by three omnidirectional wheel motors, abbreviated as IASBRR, which was proposed by Kumagai and his research team [11-12]. The studies in [9-18] established complete dynamic models and control methods of the IASBRRs in either decoupled or coupled approach, in order to achieve stabilization and trajectory tracking. The ball-riding robot also has an underactuated control problem, which is similar to a normal cart-pole inverted pendulum, which has been widely studied by numerous researchers. For the sliding model control (SMC) of uncertain IASBRRs, the authors in [15, 16, 18] proposed to exploit SMC and BLS or ORBLS to accomplish trajectory tracking control. Worthy of mention is that, through experiments, gyro stabilizer had a good effect on the suppression of external disturbance and noise. With the merits of the ORFBLS, a kind of SMC with an ORFBLS could perform better in achieving formation control of the IASBRRs .

Hence, the objectives of the paper are to propose an incremental hierarchical sliding-mode formation control method augmented with ORFBLS, or abbreviated ORFBLS-IHSMFC, and to bring forward an obstacle avoidance scheme using potential functions, in order to achieve stabilization, trajectory tracking with any collision of the multi-IASBRRs with uncertain parameters. The effectiveness and efficacy of the proposed controller will be well exemplified by conducting two simulations. The presented contents are novel in deriving the stable and ORFBLS-IHSMFC controller using Lyapunov stability theory and verifying its superiority via comparative results.

The rest of the paper is organized as follows. Section II describes the model of uncertain multi-IASBRRs, and Section III briefly describes the ORFBLS function approximation and proposes ORFBLS-IHSMFC method to achieve the goal of desired trajectory tracking control and the obstacle avoidance scheme is also raised. In Sections IV, comparative simulations are performed to illustrate the effectiveness and superiority of the ORFBLS-IHSMFC method. Section V concludes the paper.

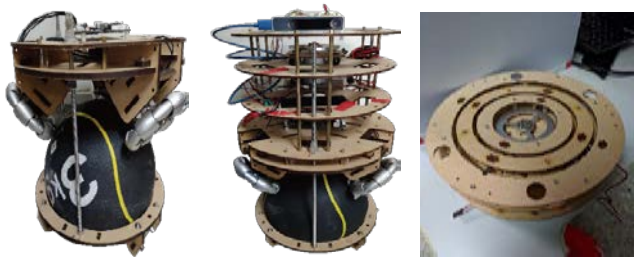

(a) (b) (c)

**Fig. 1. The experimental ball-riding robot. (a) Drive part. (b) Laboratory-built prototype. (c) Gyro-stabilizer**

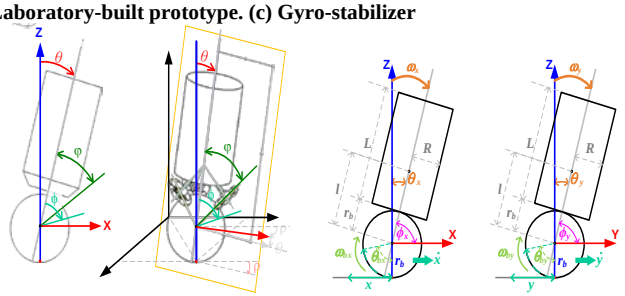

(a) (b) (c)

**Fig. 2. Illustration of the ball-riding robot. (a) The elevation angle $\theta$, the zenith angle $\varphi$. (b) The tilt angle $\theta_x$ and the motors' angular positions $\phi_x$ in the median sagittal plane. (c) The tilt angle $\theta_y$ and the motors' angular positions $\phi_y$ in the median coronal plane.**

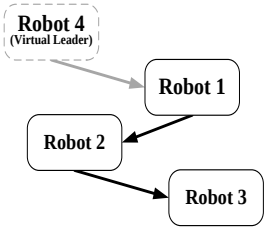


**Fig. 3. An example of communication topology.**

## II. System Structure

This section will describe the dynamic model of each IASBRR, model the multi-IASBRR system via graph theory, and then formulate the formation control problem. Fig.1 shows physical structure of each experimental ball-riding robot with a gyro-stabilizer mounted at the top of the IASBRR. The gyro-stabilizer is equipped with a high-speed rotating flywheel driven by a DC motor, as shown in Fig. 1(c). The IASBRR under consideration can be modeled by a fourth-variable nonlinear underactuated system model in the sagittal or coronal plane. Since both system models in the two planes are identical, only one-axis model is described in the following.

### *A. Dynamic Model of a Gyro-stabilized IASBRR in Formation*

The decoupled fourth-variable underactuated system model of the $i^{th}$ IASBRR in formation is modeled by (1), for $i$=1,…,$n$.

$$\begin{aligned} \dot{\theta}_i &= \omega_i \\ \dot{\omega}_i &= \ddot{\theta}_i = b_{\theta_i} u_i + g_{\theta_i} + \xi_{\theta_i} \\ \dot{x}_i &= v_i \\ \dot{v}_i &= b_{\phi_i} u_i + g_{\phi_i} + \xi_{\phi_i} \end{aligned} \tag{1}$$

where $\theta_i$, $\omega_i$, $\dot{x}_i$, $\dot{v}_i \in R^1$ are represented as the four state variables of the $i^{th}$ IASBRR, respectively, and assume that they are all directly measured and bounded; $\xi_{\theta_i}$ and $\xi_{\phi_i}$ satisfying $|\xi_{\theta i}| \le \xi_{\theta \max} < \infty$ and $|\xi_{\phi i}| \le \xi_{\phi \max} < \infty$. $g_{\theta_i}$, $g_{\phi_i}$, $b_{\theta_i}$ and $b_{\phi_i}$ are four known nonlinear scalar functions. Note that the origin is an unstable equilibrium point of system (1). Hence, the dynamics of the virtual leader is described by

$$\begin{aligned} \theta_{(n+1)} &= 0, \quad \omega_{(n+1)} = 0 \\ x_{(n+1)} &= x_d, \quad v_{(n+1)} = v_d \end{aligned} \tag{2}$$

### *B. Modeling the Multi-IASBRRs System*

Generally speaking, a multi-IASBRRs system has been regarded as a group of nonlinear dynamical systems where a leader exchanges information with other follower IASBRRs via a communication structure. A multi-IASBRRs system is composed of one virtual leader, considered as the $(n+1)^{th}$ IASBRR, and $n$ follower IASBRRs. Suppose that interconnection topology of $n$ follower IASBRRs is a directed graph $G$, and $n$ follower IASBRRs can be regarded as $n$ nodes, and the virtual leader is considered as the root. The relevant weighted adjacency matrix of the $n$ follower IASBRR s is denoted as $\mathbf{A}=[a_{ij}]$ and $a_{ij} \ge 0$, $\forall i,j \in \{1,2,\ldots,n\}$. Moreover we assume $a_{ii}=0$. The Laplacian matrix $\mathbf{L}$ of the directed graph $G$ is defined as $\mathbf{L}=\mathbf{D}-\mathbf{A}$, where $\mathbf{D}=diag(d_1,d_2,\ldots,d_n)$ and $d_i=\sum_{j=1}^{n} a_{ij}$. The interconnection topology of the overall multi- IASBRR system is follower robots with the $(n+1)$ robot as the virtual leader. In order to achieve this formation control objective, three assumptions about the communication topology are made in the following.

*Assumption 1*: The graph $\bar{G}$ with its relevant Laplacian matrix $\bar{\mathbf{L}}$ is directed and has a spanning tree with root being the virtual leader, the $(n+1)^{th}$ IASBRR.

*Assumption 2*: All of the IASBRRs are not necessarily directly connected from the leader.

*Assumption 3*: The virtual leader must be independent from every IASBRR.

According to Assumption 1, the relevant Laplacian matrix $\bar{\mathbf{L}}$ is symmetric and has only one zero eigenvalue and all other nonzero eigenvalues only have positive real part. According to Assumptions 1-3, let a diagonal matrix be denoted by $\boldsymbol{B}=diag\{a_1(n+1),\ldots,a_n(n+1)\}$, where all diagonal entries are nonnegative and it has at least one positive diagonal entry such that the summation of both matrices. Then the matrix $\boldsymbol{S}=\boldsymbol{L}+\boldsymbol{B}$, is invertible and has all the nonzero eigenvalues with positive real parts; therefore, let a positive-definite and symmetric matrix $\boldsymbol{Q}$, and a symmetric and diagonal matrix $\boldsymbol{A}$ such that $\boldsymbol{AS}+\boldsymbol{S}^T\boldsymbol{A}=\boldsymbol{Q}$. In addition, the matrix $\boldsymbol{A}=diag\{a_1,\ldots,a_n\}$, and $[1/a_1,\ldots,1/a_n]^T=\boldsymbol{S}^{-1}[1,\ldots,1]^T$.

### *C. Problem Statement*

In this subsection, let us consider a mission that n follower IASBRRs track their leader's trajectory, and both the IASBRRs (robots) and the leader form in formation as shown in Fig. 2(b). In order to achieve this mission, its control objective is defined as follows: Each of the IASBRRs follows their leader's trajectory, and the state variables asymptotically converges to the desired state variables of the $i^{th}$ IASBRR. This is formulated as $\lim_{t\to\infty} \theta_i(t) = \lim_{t\to\infty} \omega_i(t) = 0$, $\lim_{t\to\infty} \left( x_i(t) - x_i^*(t) \right) = 0$,

$\lim_{t\to\infty}\left(v_i(t)-v_i^*(t)\right)=0$ , $i\in\{1,2,\ldots,n+1\}$, where $x_i^*(t)=x_L(t)+f_i(t)$ and $v_i^*(t)=\dot{x}_L(t)$ are respectively denoted by the desired responses and $f_i(t)$ is the ideal relative position between the $i^{th}$ IASBRR and leader, namely that asymptotical consensus tracking can be achieved.

*Assumption 4*: $x_L(t)$ and $f_i(t)$, $i=1,\ldots,n$, are twice differentiable. $f_i(t)$, $\dot{f}_i(t)$ and $\ddot{f}_i(t)$, are known for the $i^{th}$ IASBRR.

*Assumption 5*: All the state variables of the $i^{th}$ IASBRR are directly measured.

## III. ORFBLS Function Approximator and Controller Design

### A. Introduction to ORFBLS

The structure of the Output Recurrent Fuzzy BLS (ORFBLS) is depicted in Fig. 4. There are five layers in this network: Input layer, Fuzzy subsystem layer, Defuzzification layer, Enhancement layer, and output layer, and Output layer will send a recurrent. Function of each layers are described in the following.

(1) **Input layer:** Every node in the input layer directly transfers its input to its output. There are totally $m$ nodes in the input layer, $x_i$, $i=1\sim m$.

(2) **Fuzzy subsystem layer:** There are totally $N_1$ fuzzy subsystems in the Fuzzy subsystem layer and each subsystem has $M_s$, $s=1\sim N_1$ fuzzy rules. The membership function is given by an exponential function written as

$$\mu_{ri}^s=\exp[-((x_i-c_{ri}^s)/(\sigma_{ri}^s))^2] \tag{3}$$

where $i=1\sim m$, $r=1\sim M_s$, $c^s_{ri}$ and $\sigma^s{}_{ri}{}^2$ are mean and variance of the membership function, respectively. The weighted output of each rule is written as

$$z_r^s=w_r^s\alpha_r^s\ ,\ \text{where}\ \begin{cases} w_r^s=\tau_r^s\Big/\sum_{r=1}^{M_s}\tau_r^s \\ \tau_r^s=\prod_{i=1}^{m}\mu_{ri}^s \end{cases} \tag{4}$$

The output of the fuzzy subsystem layer is $\mathbf{Z}=\left[\mathbf{z}_1,.....,\mathbf{z}_{N_1}\right]_{1\times\left(M_1+M_2+\cdots+M_{N_1}\right)}$, and $\mathbf{z}_s=[z_1^s,.....,z_{M_s}^s]_{1\times M_s}$ is the output of the $s^{th}$ fuzzy subsystem.

(3) **Defuzzification layer:** The output of each node in the defuzzification layer is the summarization of the outputs of the corresponding fuzzy subsystem. Hence, for each node, the output is given by

$$y_s^{(\mathrm{def})}=\sum_{r=1}^{M_s}z_r^s \tag{5}$$

and the output of the defuzzification layer is $\mathbf{y}_{\mathrm{def}}:[y_1^{(\mathrm{def})},.....,y_{N_1}^{(\mathrm{def})}]$.

(4) **Enhancement layer:** This layer is with $N_2$ group of neurons and totally $H_2$ nodes. The input of this layer is $\mathbf{Z}:[\mathbf{z}_1,.....,\mathbf{z}_{N_1}]$, $\mathrm{y_{out}}(\mathrm{t\text{-}1})$ form the fuzzy subsystem layer, and the output of this layer is

$$\mathbf{y}_{\mathrm{enh}}=\phi(\boldsymbol{x}^{(\mathrm{enh})}) \tag{6}$$

where

$$\boldsymbol{x}^{(\mathrm{enh})}=\mathbf{Z}\mathbf{W}^{(\mathrm{sub})}+\boldsymbol{\beta}+\mathbf{W}^{(\mathrm{out})}\mathrm{y_{out}}(\mathrm{t}-1) \tag{7}$$

and

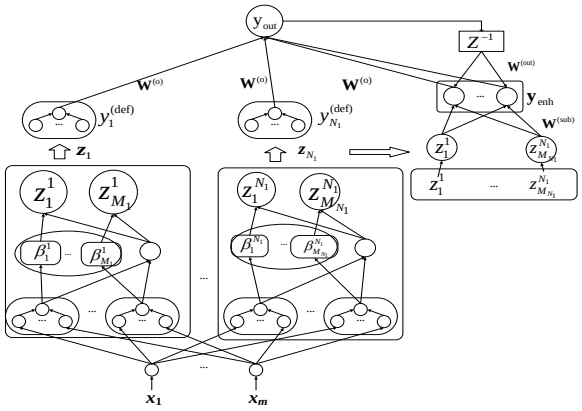


**Fig. 4. System Structure of the ORFBLS.**

$\mathbf{Z}\in R^{1\times(M_1+M_2+\cdots+M_{N_1})}$ $\mathbf{W}^{(\mathrm{sub})}\in R^{(M_1+M_2+\cdots+M_{N_1})\times H_2}$

$\boldsymbol{\beta}\in R^{1\times H_2}$ $\mathbf{W}^{(\mathrm{out})}\in R^{1\times H_2}$

(5) **Output layer:** The input of the output layer is formulated as follows:

$$\boldsymbol{x}^{(\mathrm{o})}=[\mathbf{y}_{\mathrm{def}},\mathbf{y}_{\mathrm{enh}}]^T \tag{8}$$

Then the output of the output layer is the weighted sum of its input and can be described as

$$\mathrm{y_{out}}=\mathbf{W}^{(\mathrm{o})}\boldsymbol{x}^{(\mathrm{o})} \tag{9}$$

where $\mathbf{W}^{(\mathrm{o})}$ is the weight to be learned and $\mathrm{y_{out}}$ is the output of the ORFBLS.

Let the ideal approximation result of the ORFBLS be

$$y_{\mathrm{out}}{}^*=\mathbf{W}^{*(\mathrm{o})}\boldsymbol{x}^{*(\mathrm{o})}+\varepsilon^* \tag{10}$$

where $\mathbf{W}^{*(\mathrm{o})}$ is the optimal weight vector; $\boldsymbol{x}^{*(o)}$ is the optimal input of the output layer; than a small and bounded error vector denoted as $\varepsilon^*$. The parameters, $\boldsymbol{\sigma}$, $\boldsymbol{\alpha}$, and $\mathbf{c}$, the weights and bias of the ORFBLS, $\mathbf{W}^{(\mathrm{sub})}$, $\mathbf{W}^{(\mathrm{out})}$, $\boldsymbol{\beta}$ and $\mathbf{W}^{(\mathrm{o})}$ are waited to be determined. Note that the norms of the optical weights and bias $\left\|\boldsymbol{\sigma}^*\right\|,\left\|\boldsymbol{\alpha}^*\right\|,\left\|\mathbf{c}^*\right\|,\left\|\mathbf{W}^{*(\mathrm{sub})}\right\|,\left\|\mathbf{W}^{*(\mathrm{out})}\right\|,\left\|\boldsymbol{\beta}^*\right\|$ and $\left\|\mathbf{W}^{*(\mathrm{o})}\right\|$ are bounded. Let $\hat{\boldsymbol{\sigma}},\hat{\boldsymbol{\alpha}},\hat{\mathbf{c}},\hat{\mathbf{W}}^{(\mathrm{sub})},\hat{\mathbf{W}}^{(\mathrm{out})}$, $\hat{\boldsymbol{\beta}}$ and $\hat{\mathbf{W}}^{(\mathrm{o})}$ be the estimations of $\boldsymbol{\sigma}^*$, $\boldsymbol{\alpha}^*$, $\mathbf{c}^*$, $\mathbf{W}^{*(\mathrm{sub})}$, $\mathbf{W}^{*(\mathrm{out})}$, $\boldsymbol{\beta}^*$, $\mathbf{W}^{*(\mathrm{o})}$, and the estimation errors equals to difference between the optimal values and the estimation values. Hence, rewriting (9) gives

$$\begin{aligned} y_{\mathrm{out}} &= (\tilde{\mathbf{W}}^{(\mathrm{o})}+\hat{\mathbf{W}}^{(\mathrm{o})})(\tilde{\boldsymbol{x}}^{(\mathrm{o})}+\hat{\boldsymbol{x}}^{(\mathrm{o})})+\varepsilon \\ &= \hat{\mathbf{W}}^{(\mathrm{o})}\hat{\boldsymbol{x}}^{(\mathrm{o})}+\tilde{\mathbf{W}}^{(\mathrm{o})}\hat{\boldsymbol{x}}^{(\mathrm{o})}+\hat{\mathbf{W}}^{(\mathrm{o})}\tilde{\boldsymbol{x}}^{(\mathrm{o})}+\varepsilon_r \end{aligned} \tag{11}$$

in which $\hat{y}_{\mathrm{out}}=\hat{\mathbf{W}}^{(\mathrm{o})}\hat{\boldsymbol{x}}^{(\mathrm{o})}$ , $\varepsilon_r=\tilde{\mathbf{W}}^{(\mathrm{o})}\tilde{\boldsymbol{x}}^{(\mathrm{o})}+\varepsilon$ . Expanding $\tilde{\boldsymbol{x}}^{(\mathrm{o})}$ by Taylor Series obtains

$$\begin{aligned} \tilde{\boldsymbol{x}}^{(\mathrm{o})} &= \left(\frac{\partial\hat{\boldsymbol{x}}^{(\mathrm{o})}}{\partial\hat{\mathbf{W}}^{(\mathrm{enh})}}\right)\tilde{\mathbf{W}}^{(\mathrm{enh})}+\left(\frac{\partial\hat{\boldsymbol{x}}^{(\mathrm{o})}}{\partial\hat{\mathbf{W}}^{(\mathrm{out})}}\right)\tilde{\mathbf{W}}^{(\mathrm{out})} \\ &+\left(\frac{\partial\hat{\boldsymbol{x}}^{(\mathrm{o})}}{\partial\hat{\mathbf{W}}^{(\mathrm{sub})}}\right)\tilde{\mathbf{W}}^{(\mathrm{sub})}+\left(\frac{\partial\hat{\boldsymbol{x}}^{(\mathrm{o})}}{\partial\hat{\boldsymbol{\sigma}}}\right)\tilde{\boldsymbol{\sigma}}+\left(\frac{\partial\hat{\boldsymbol{x}}^{(\mathrm{o})}}{\partial\hat{\boldsymbol{\alpha}}}\right)\tilde{\boldsymbol{\alpha}} \\ &+\left(\frac{\partial\hat{\boldsymbol{\beta}}}{\partial\hat{\boldsymbol{\beta}}}\right)\tilde{\boldsymbol{\beta}}+\left(\frac{\partial\hat{\boldsymbol{x}}^{(\mathrm{o})}}{\partial\hat{\mathbf{c}}}\right)\tilde{\mathbf{c}}+\tilde{\mathbf{h}} \end{aligned} \tag{12}$$

Therefore, the approximation errors of the FBLS can be expressed as

$$\begin{aligned}\tilde{y}_{\text{out}} &= \tilde{\mathbf{W}}^{(\text{o})}\hat{\boldsymbol{x}}^{(\text{o})} + \hat{\mathbf{W}}^{(\text{o})}\left(\frac{\partial\hat{\boldsymbol{x}}^{(\text{o})}}{\partial\hat{\mathbf{W}}^{(\text{enh})}}\right)\tilde{\mathbf{W}}^{(\text{enh})} \\ &+ \hat{\mathbf{W}}^{(\text{o})}\left(\frac{\partial\hat{\boldsymbol{x}}^{(\text{o})}}{\partial\hat{\mathbf{W}}^{(\text{out})}}\right)\tilde{\mathbf{W}}^{(\text{out})} + \hat{\mathbf{W}}^{(\text{o})}\left(\frac{\partial\hat{\boldsymbol{x}}^{(\text{o})}}{\partial\hat{\mathbf{W}}^{(\text{sub})}}\right)\tilde{\mathbf{W}}^{(\text{sub})} \\ &+ \hat{\mathbf{W}}^{(\text{o})}\left(\frac{\partial\hat{\boldsymbol{x}}^{(\text{o})}}{\partial\hat{\boldsymbol{\sigma}}}\right)\tilde{\boldsymbol{\sigma}} + \hat{\mathbf{W}}^{(\text{o})}\left(\frac{\partial\hat{\boldsymbol{x}}^{(\text{o})}}{\partial\hat{\boldsymbol{\alpha}}}\right)\tilde{\boldsymbol{\alpha}} \\ &+ \hat{\mathbf{W}}^{(\text{o})}\left(\frac{\partial\hat{\boldsymbol{x}}^{(\text{o})}}{\partial\hat{\boldsymbol{\beta}}}\right)\tilde{\boldsymbol{\beta}} + \hat{\mathbf{W}}^{(\text{o})}\left(\frac{\partial\hat{\boldsymbol{x}}^{(\text{o})}}{\partial\hat{\mathbf{c}}}\right)\tilde{\mathbf{c}} + h\end{aligned} \tag{13}$$

where $h = \hat{\mathbf{W}}^{(\text{o})}\tilde{\mathbf{h}} + \varepsilon_r$, and $h$ is assumed bounded, i,e., $0 \le \|h\| < h_{\max} < \infty$

*B. Proposed ORFBLS-IHSMFC Motion Control*

This section will present the procedures of designing the proposed ORFBLS-IHSM formation controller, abbreviated as ORFBLS-IHSMFC, for tracking $\phi_x^*$, $\phi_y^*$, $\dot{\phi}_x^*(t)$, $\dot{\phi}_y^*(t)$ and stabilizing all variables $\theta_x$, $\theta_y$, $\dot{\theta}_x(t)$ and $\dot{\theta}_y(t)$ at $\theta_x^*$, $\theta_y^*$, $\dot{\theta}_x^*(t)$ and $\dot{\theta}_y^*(t)$, respectively. Since the dynamic equations of motion of the robot in both sagittal and coronal planes are identical except the notations. Hence, only the controller in the sagittal plane is designed during the two steps controller design process.

**Step 1:** the first step defines a tracking error and constructs the sliding surface. Define the tracking errors vectors by:

$$\mathbf{e}_1 = \boldsymbol{\theta} - \boldsymbol{\theta}^* \tag{14}$$

$$\mathbf{e}_2 = \dot{\boldsymbol{\theta}} - \dot{\boldsymbol{\theta}}^* \tag{15}$$

Thus, the derivative of the tracking errors is

$$\dot{\mathbf{e}}_1 = \mathbf{e}_2 \tag{16}$$

$$\dot{\mathbf{e}}_2 = \mathbf{b}_\theta(\mathbf{e}_1, \mathbf{e}_2)\mathbf{u} + \mathbf{g}_\theta(\mathbf{e}_1, \mathbf{e}_2) + \xi_\theta \tag{17}$$

**Step 2:** the second step defines the consensus state errors of ballbot i.

$$e_{3i} = \sum_{j=1}^{n+1} a_{ij}(\overline{x}_i - \overline{x}_j) \tag{18}$$

$$e_{4i} = \sum_{j=1}^{n+1} a_{ij}(\dot{\overline{x}}_i - \dot{\overline{x}}_j) \tag{19}$$

Hence, the consensus state errors of n ballbots is

$$\mathbf{e}_3 = (\boldsymbol{S}_G \otimes \mathbf{I}_1)(\mathbf{x} - \mathbf{x}^*) \tag{20}$$

$$\mathbf{e}_4 = (\boldsymbol{S}_G \otimes \mathbf{I}_1)(\dot{\mathbf{x}} - \dot{\mathbf{x}}^*) = (\boldsymbol{S}_G \otimes \mathbf{I}_1)(\mathbf{v} - \mathbf{v}^*) \tag{21}$$

Than, the derivative of the consensus state errors is

$$\dot{\mathbf{e}}_3 = \mathbf{e}_4 \tag{22}$$

$$\dot{\mathbf{e}}_4 = (\boldsymbol{S}_G \otimes \mathbf{I}_1)(\dot{\mathbf{v}} - \dot{\mathbf{v}}^*) = \boldsymbol{S}_G\left(\mathbf{b}_\phi\mathbf{u} + \mathbf{g}_\phi + \xi_\phi - \ddot{\mathbf{x}}^*\right) \tag{23}$$

In order to make all error vectors steadily approach zero, it is necessary to construct the subsequent sliding surface by following the design process of the incremental hierarchical sliding-mode controller in [14],

$$\boldsymbol{S}_1 = \mathbf{k}_1\mathbf{e}_1 + \mathbf{e}_2 \tag{24}$$

$$\boldsymbol{S}_2 = \mathbf{k}_2\mathbf{e}_3 + \boldsymbol{S}_1 \tag{25}$$

$$\boldsymbol{S}_3 = \mathbf{k}_3\mathbf{e}_4 + \boldsymbol{S}_2 \tag{26}$$

where $\mathbf{k}_1$, $\mathbf{k}_2$, $\mathbf{k}_3$ are three diagonal matrices and their diagonal elements, $k_{1ii} = \overline{k}_1 > 0$, ; $k_{2ii} = \overline{k}_2\,\text{sgn}(s_{1i}e_{3i})$ $\overline{k}_2 > 0$ ; $k_{3ii} = \overline{k}_3\,\text{sgn}(s_{2i}e_{4i})$, $\overline{k}_3 > 0$. Thus $\boldsymbol{S}_3$ becomes

$$\boldsymbol{S}_3 = \mathbf{k}_3\mathbf{e}_4 + \mathbf{k}_2\mathbf{e}_3 + \mathbf{k}_1\mathbf{e}_1 + \mathbf{e}_2 \tag{27}$$

From (24-27), it implies that $|\boldsymbol{S}_3| \ge |\boldsymbol{S}_2| \ge |\boldsymbol{S}_1| \ge 0$. Considering the uncertainty terms $\xi_\theta, \xi_\phi$, the time derivative of the sliding surface $\boldsymbol{S}_3$ is given by

$$\dot{\boldsymbol{S}}_3 = \mathbf{k}_3\mathrm{S}_G\left(\mathbf{b}_\phi\mathbf{u} + \mathbf{g}_\phi - \ddot{\mathbf{x}}^*\right) + \mathbf{k}_2\mathbf{e}_4 + \mathbf{k}_1\mathbf{e}_2 + \mathbf{b}_\theta\mathbf{u} + \mathbf{g}_\theta + \boldsymbol{\xi} \tag{28}$$

where $\boldsymbol{\xi} = \mathbf{k}_3\boldsymbol{S}_G\xi_\phi + \xi_\theta \equiv [\xi_1, \xi_2, ...., \xi_n]^T$. Let the control law be $\mathbf{u} = \mathbf{u}_{eq} + \mathbf{u}_{sw} + \mathbf{u}_\xi$, the equivalent and switching control, respectively. The equivalent control $\mathbf{u}_{eq}$ can be found such that $\dot{\boldsymbol{S}}_3 = 0$,

$$\mathbf{u}_{eq} = \frac{1}{\mathbf{k}_3\boldsymbol{S}_G\mathbf{b}_\phi + \mathbf{b}_\theta}\left(\mathbf{k}_3\boldsymbol{S}_G\left(\ddot{\mathbf{x}}^* - \mathbf{g}_\phi\right) - \left(\mathbf{k}_2\mathbf{e}_4 + \mathbf{k}_1\mathbf{e}_2 + \mathbf{g}_\theta\right)\right) \tag{29}$$

$$\mathbf{u}_{sw} = \frac{-1}{\mathbf{k}_3\boldsymbol{S}_G\mathbf{b}_x + \mathbf{b}_\theta}\left(k_4\boldsymbol{S}_3 + k_5\text{sgn}\left(\boldsymbol{S}_3\right)\right) \tag{30}$$

$$\mathbf{u}_\xi = -\left(\mathbf{k}_3\boldsymbol{S}_G\mathbf{b}_x + \mathbf{b}_\theta\right)^{-1}\hat{\boldsymbol{\xi}} \tag{31}$$

where $\hat{\boldsymbol{\xi}}$ is the real output of the used ORFBLS, and $\dot{\boldsymbol{S}}_3$ becomes

$$\dot{\boldsymbol{S}}_3 = -k_4\boldsymbol{S}_3 - k_5\text{sgn}(\boldsymbol{S}_3) + \tilde{\boldsymbol{\xi}} \tag{32}$$

In order to prove the stability of the controller, the Lyapunov function is chosen by

$$\begin{aligned}V &= \frac{1}{2}\boldsymbol{S}_3{}^T\boldsymbol{S}_3 + \sum_{i=1}^{n}\frac{1}{2r_{\mathbf{W}_i^{(\text{o})}}}\tilde{\mathbf{W}}_i^{(\text{o})^T}\tilde{\mathbf{W}}_i^{(\text{o})} \\ &+ \sum_{i=1}^{n}\frac{1}{2r_{\mathbf{W}_i^{(\text{enh})}}}\tilde{\mathbf{W}}_i^{(\text{enh})^T}\tilde{\mathbf{W}}_i^{(\text{enh})} + \sum_{i=1}^{n}\frac{1}{2r_{\mathbf{W}_i^{(\text{sub})}}}\tilde{\mathbf{W}}_i^{(\text{sub})^T}\tilde{\mathbf{W}}_i^{(\text{sub})} \\ &+ \sum_{i=1}^{n}\frac{1}{2r_{\mathbf{W}_i^{(\text{out})}}}\tilde{\mathbf{W}}_i^{(\text{out})^T}\tilde{\mathbf{W}}_i^{(\text{out})} + \sum_{i=1}^{n}\frac{1}{2r_{\boldsymbol{\sigma}_i}}\tilde{\boldsymbol{\sigma}}_i{}^T\tilde{\boldsymbol{\sigma}}_i \\ &+ \sum_{i=1}^{n}\frac{1}{2r_{\boldsymbol{\alpha}_i}}\tilde{\boldsymbol{\alpha}}_i{}^T\tilde{\boldsymbol{\alpha}}_i + \sum_{i=1}^{n}\frac{1}{2r_{\mathbf{c}_i}}\tilde{\mathbf{c}}_i{}^T\tilde{\mathbf{c}}_i + \sum_{i=1}^{n}\frac{1}{2r_{\boldsymbol{\beta}_i}}\tilde{\boldsymbol{\beta}}_i{}^T\tilde{\boldsymbol{\beta}}_i\end{aligned} \tag{33}$$

Since the time derivative of $V$ is expressed by

$$\begin{aligned}\dot{V} &= -k_4\boldsymbol{S}_3{}^T\boldsymbol{S}_3 - k_5\|\boldsymbol{S}_3\|_1 + \sum_{i=1}^{n}\tilde{\mathbf{W}}_i^{(\text{o})^T}[S_{3i}{}^T\hat{\boldsymbol{x}}_i^{(\text{o})} - \frac{\dot{\hat{\mathbf{W}}}_i^{(\text{o})}}{r_{\mathbf{W}_i^{(\text{o})}}}] \\ &+ \sum_{i=1}^{n}\tilde{\mathbf{W}}_i^{(\text{enh})^T}[S_{3i}{}^T\left(\frac{\partial\hat{\boldsymbol{x}}_i^{(\text{o})}}{\partial\hat{\mathbf{W}}_i^{(\text{enh})}}\right)^T\hat{\mathbf{W}}_i^{(\text{o})} - \frac{\dot{\hat{\mathbf{W}}}_i^{(\text{enh})}}{r_{\mathbf{W}_i^{(\text{enh})}}}] \\ &+ \sum_{i=1}^{n}\tilde{\mathbf{W}}_i^{(\text{sub})^T}[S_{3i}{}^T\left(\frac{\partial\hat{\boldsymbol{x}}_i^{(\text{o})}}{\partial\hat{\mathbf{W}}_i^{(\text{sub})}}\right)^T\hat{\mathbf{W}}_i^{(\text{o})} - \frac{\dot{\hat{\mathbf{W}}}_i^{(\text{sub})}}{r_{\mathbf{W}_i^{(\text{sub})}}}] \\ &\square\boxplus\sum_{i=1}^{n}\tilde{\mathbf{W}}_i^{(\text{out})^T}[S_{3i}{}^T\left(\frac{\partial\hat{\boldsymbol{x}}_i^{(\text{o})}}{\partial\hat{\mathbf{W}}_i^{(\text{out})}}\right)^T\hat{\mathbf{W}}_i^{(\text{o})} - \frac{\dot{\hat{\mathbf{W}}}_i^{(\text{out})}}{r_{\mathbf{W}_i^{(\text{out})}}}] \\ &\boxplus\sum_{i=1}^{n}\tilde{\boldsymbol{\sigma}}_i{}^T[S_{3i}{}^T\left(\frac{\partial\hat{\boldsymbol{x}}_i^{(\text{o})}}{\partial\hat{\boldsymbol{\sigma}}_i}\right)^T\hat{\mathbf{W}}_i^{(\text{o})} - \frac{\dot{\hat{\boldsymbol{\sigma}}}_i}{r_{\boldsymbol{\sigma}_i}}] + \sum_{i=1}^{n}\tilde{\boldsymbol{\alpha}}_i{}^T[S_{3i}{}^T\left(\frac{\partial\hat{\boldsymbol{x}}_i^{(\text{o})}}{\partial\hat{\boldsymbol{\alpha}}_i}\right)^T\hat{\mathbf{W}}_i^{(\text{o})} - \frac{\dot{\hat{\boldsymbol{\alpha}}}_i}{r_{\boldsymbol{\alpha}_i}}] \\ &+ \sum_{i=1}^{n}\tilde{\mathbf{c}}_i{}^T[S_{3i}{}^T\left(\frac{\partial\hat{\boldsymbol{x}}_i^{(\text{o})}}{\partial\hat{\mathbf{c}}_i}\right)^T\hat{\mathbf{W}}_i^{(\text{o})} - \frac{\dot{\hat{\mathbf{c}}}_i}{r_{\mathbf{c}_i}}]\end{aligned} \tag{34}$$

$$\square\square\square\boxplus\sum_{i=1}^{n}\tilde{\boldsymbol{\beta}}_i^T[S_{3i}^T\left(\frac{\partial\hat{\boldsymbol{x}}_i^{(o)}}{\partial\hat{\boldsymbol{\beta}}_i}\right)^T\hat{\mathbf{W}}_i^{(o)}-\frac{\dot{\hat{\boldsymbol{\beta}}}_i}{r_{\boldsymbol{\beta}_i}}]+\boldsymbol{S}_3^T\mathbf{h}$$

let us choose the following parameters update laws

$$\dot{\hat{\mathbf{W}}}_i^{(o)}=r_{\mathbf{W}_i^{(o)}}S_{3i}^T\hat{\boldsymbol{x}}_i^{(o)},\ \dot{\hat{\mathbf{W}}}_i^{(enh)}=r_{\mathbf{W}_i^{(enh)}}S_{3i}^T\left(\frac{\partial\hat{y}_{iout}}{\partial\hat{\mathbf{W}}_i^{(enh)}}\right)^T$$

$$\dot{\hat{\mathbf{W}}}_i^{(sub)}=r_{\mathbf{W}_i^{(sub)}}S_{3i}^T\left(\frac{\partial\hat{y}_{iout}}{\partial\hat{\mathbf{W}}_i^{(sub)}}\right)^T$$

$$\dot{\hat{\mathbf{W}}}_i^{(out)}=r_{\mathbf{W}_i^{(out)}}S_{3i}^T\left(\frac{\partial\hat{y}_{iout}}{\partial\hat{\mathbf{W}}_i^{(out)}}\right)^T \tag{35}$$

$$\dot{\hat{\boldsymbol{\sigma}}}_i=r_{\boldsymbol{\sigma}_i}S_{3i}^T\left(\frac{\partial\hat{y}_{iout}}{\partial\hat{\boldsymbol{\sigma}}_i}\right)^T,\dot{\hat{\boldsymbol{\alpha}}}_i=r_{\boldsymbol{\alpha}_i}S_{3i}^T\left(\frac{\partial\hat{y}_{iout}}{\partial\hat{\boldsymbol{\alpha}}_i}\right)^T$$

$$\dot{\hat{\boldsymbol{\beta}}}_i=r_{\boldsymbol{\beta}_i}S_{3i}^T\left(\frac{\partial\hat{y}_{iout}}{\partial\hat{\boldsymbol{\beta}}_i}\right)^T,\ \dot{\hat{\mathbf{c}}}_i=r_{\mathbf{c}_i}S_{3i}^T\left(\frac{\partial\hat{y}_{iout}}{\partial\hat{\mathbf{c}}_i}\right)^T$$

With the aforementioned parameter adjustment laws, the time derivative of the Lyapunov function becomes

$$\dot{V}\le-k_4\boldsymbol{S}_3^T\boldsymbol{S}_3-(k_5-h_{\max})\|\boldsymbol{S}_3\| \tag{36}$$

Therefore, it turns out

$$\dot{V}\le 0,\ \text{if}\ k_5>h_{\max} \tag{37}$$

Since $\dot{V}$ are negative semi-definite, it is easy to show via Lyapunov stability theory and the generalized LaSalle's invariance principle that the sliding function $\boldsymbol{S}_3$ converges to the origin asymptotically, and since $V_1=\boldsymbol{S}_1^T\boldsymbol{S}_1/2\ \le\ V_2=\boldsymbol{S}_2^T\boldsymbol{S}_2/2\ \le\ V_3=\boldsymbol{S}_3^T\boldsymbol{S}_3/2\ \to 0$, thus implying $\boldsymbol{S}_2$ and $\boldsymbol{S}_1$ tend to zero asymptotically. This shows that $\mathbf{e}_1,\mathbf{e}_2,\mathbf{e}_3$ and $\mathbf{e}_4$ approach zero as time goes to infinity.

*C. Obstacle Avoidance Using Potential function*

The basic idea behind the collision-avoidance policy is that the robots must take evasive action in the working space if there are possible risks of collisions among the robots. The repulsive potential energy is given by

$$U(q_i)=U_{ca}(q_i)+U_{oa}(q_i) \tag{38}$$

where $U_{ca}(q_i)$ and $U_{oa}(q_i)$ are repulsive potential of collision avoidance and obstacle avoidance, respectively. $i$, $j$=1, 2,$\cdots$,$n$ is the number of robot, and k is the number of obstacle.

$$U_{ca}(q_i)=\begin{cases}\frac{1}{2}K_{ca}\sum_{j=1,i\ne j}^{n}(\frac{1}{\rho(q_{ij})}-\frac{1}{\rho_0})^2 & \text{if}\ \rho(q_{ij})\le\rho_0\\ 0 & \text{if}\ \rho(q_{ij})>\rho_0\end{cases} \tag{39}$$

$$U_{oa}(q_i)=\begin{cases}\frac{1}{2}K_{oa}\sum_{k=1}^{M}(\frac{1}{\rho(q_{ik})}-\frac{1}{\rho_0})^2 & \text{if}\ \rho(q_{ik})\le\rho_0\\ 0 & \text{if}\ \rho(q_{ik})>\rho_0\end{cases} \tag{40}$$

where $\rho(q_{ik})$ and $\rho_0$ are the minimum distance to the obstacle and safe region, respectively. From (39-40), we have the repulsive force to avoid the obstacle as below.

$$\mathbf{u}_{co_i}=-\nabla U(q_i)=\left[-\frac{\partial U(q_i)}{\partial q_i}^T,0\right]^T=\mathbf{u}_{ca_i}+\mathbf{u}_{oa_i}\in R^3 \tag{41}$$

**TABLE I.**

**THE AVERAGED EXECUTION TIME AND PERFORMANCE INDEXES OF THE PROPOSED METHOD AND CONTROLLER.**

| Performance index | ORFBLS-IHSMFC | ORBLS-BSMFC | BLS-BSMFC |
|---|---|---|---|
| ISE (Circle) | 129.1959 | 129.4548 | 130.5008 |
| IAE (Circle) | 33.0040 | 33.4387 | 37.7815 |
| ITAE (Circle) | 488.7595 | 495.1971 | 615.7238 |
| ITSE (Circle) | 330.0210 | 330.2852 | 378.0419 |
| ISE (Line) | 8.2087 | 8.4412 | 9.094033 |
| IAE (Line) | 7.2181 | 7.7614 | 6.431333 |
| ITAE (Line) | 27.5195 | 29.9125 | 36.2215 |
| ITSE (Line) | 10.8040 | 11.0583 | 17.29477 |
| ISE(p2p) | 16.2125 | 16.3041 | 21.3659 |
| IAE(p2p) | 9.3346 | 9.5369 | 12.8473 |
| ITAE(p2p) | 28.1191 | 30.4948 | 32.8825 |
| ITSE(p2p) | 23.7519 | 24.4264 | 28.1257 |

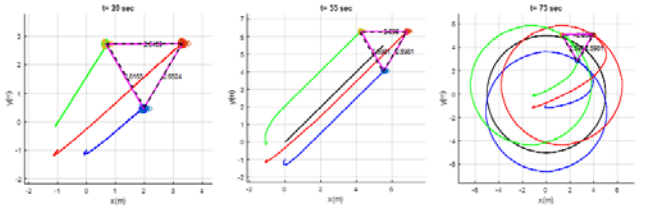

**(a) (b) (c)**

**Fig.5. Simulation results of formation control of the three IASBRRs using the proposed ORBLS-BSMFC. (a) Point-to-point stabilization. (b) Line tracking. (c) Circular tracking formation trajectories.**

where

$$\boldsymbol{u}_{ca_i}=\begin{cases}K_{ca}\sum_{j=1}^{n}(\frac{1}{\rho(q_{ij})}-\frac{1}{\rho_0})\frac{1}{\rho^2(q_{ij})}\frac{q_i-q_j}{\rho(q_{ij})} & \text{if}\ \rho(q_{ij})\le\rho_0\\ 0 & \text{if}\ \rho(q_{ij})>\rho_0\end{cases}$$

$$\boldsymbol{u}_{oa_i}=\begin{cases}K_{oa}\sum_{k=1}^{M}(\frac{1}{\rho(q_{ik})}-\frac{1}{\rho_0})\frac{1}{\rho^2(q_{ik})}\frac{q_i-q_{obstacle}^k}{\rho(q_{ik})} & \text{if}\ \rho(q_{ik})\le\rho_0\\ 0 & \text{if}\rho(q_{ik})>\rho_0\end{cases}$$

Hence, the modified motion trajectory is given by

$$\mathrm{P}_{doa}=\mathrm{P}_d+\mathrm{u}_{co_i} \tag{42}$$

where $\mathrm{P}_{doa}$ is the modified trajectory of any IASBRR.

## IV. SIMULATIONS AND DISCUSSION

In order to examine the performance and merit of the proposed ORFBLS-IHSMFC controller together with the obstacle avoidance method, three simulations in this section are conducted. The first simulation is carried out to investigate the comparative performance of the proposed ORFBLS-IHSMFC for point-to-point stabilization, straight line and circular tracking. The last two simulations are performed to show the effectiveness of the proposed ORFBLS-IHSMFC controller together with the obstacle avoidance method. Three simulations adopt the communication topology as shown in Fig. 1(a). In the beginning of both simulations, one sliding-mode value is initially selected to enable the ORFBLS to estimate the uncertainty. The number of inputs, fuzzy subsystem layer, enhancement nodes and outputs of the ORFBLS are respectively set by 4, 5, 5 and 1, respectively. All the learning parameters, $r_{\mathbf{W}^{(o)}}$, $r_{\mathbf{W}^{(enh)}}$, $r_{\mathbf{W}^{(out)}}$, $r_{\boldsymbol{\alpha}}$, $r_{\boldsymbol{\beta}}$ and $r_{\mathbf{c}}$ for the

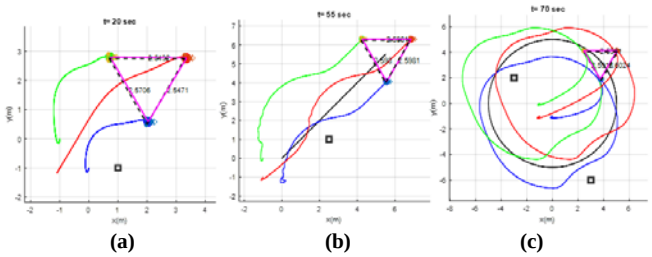

(a) (b) (c)

**Fig. 6. Simulation results of the formation tracking strategy via the proposed ORBLS-BSMFC and obstacle avoidance method. (a) Point-to-point stabilization. (b)Line tracking. (c)Circle tracking.**

three FBLSs in (41) are the same and equal to 0.05. Both simulations are executed using Matlab/Simulink and the proposed controller is executed with $\bar{k}_1 = 2$, $\bar{k}_2 = 0.3467$, $\bar{k}_3 = 0.8667$, $k_4 = 10.5$, $k_5 = 5.5$.

The first simulation is done to achieve the triangular formation. Fig. 5 shows the simulation results of formation control of the three IASBRRs using the proposed ORFBLS-IHSMFC. Table I compares the comparative performance indexes of the proposed ORFBLS-IHSMFC method and two existing methods: ORBLS-BSMFC [16] and BLS-BSMFC[18]. From the comparative results in the triangular formation, the proposed ORFBLS-IHSMFC method significantly outperforms the two existing methods in terms of the ISE, IAE, ITAE and ITSE for point-to-point stabilization, straight line and circular tracking.

The second simulation aims to control the three IASBRRs in triangular formation to move along a desired trajectory in which obstacles are located in the moving path. In Fig. 6, the black dotted triangle denotes the desire formation, and the center is the virtual leader. During the obstacle avoidance process, the strategy adopted is that the formation is not allowed to be destroyed. In doing so, obstacle detection is performed in the virtual leader, and the entire team must be kept in formation while encountering obstacles. This strategy is particularly useful in transporting heavy objects by using a team of ball-riding robots. Fig. 6 shows the simulation results of the proposed formation tracking strategy and obstacle avoidance methods for point-to-point stabilization, tracking straight line and circular movement of the leader. The results in Fig. 6 reveals that the three robots move in formation and avoiding the obstacle, showing the effectiveness of the proposed method for cooperative transportation.

## V. Conclusions and Future Work

This paper has presented a novel ORFBLS-IHSMFC method together with an obstacle avoidance scheme for formation control of a team of uncertain IASBRRs with gyro stabilizers. The ORFBLS-IHSMFC has been derived and proven using the Lyapunov stability theory, in order to achieve formation control as well as stabilization and trajectory tracking in presence of parameter variations, such as mass, inertia and frictions. The ORFBLS-IHSMFC has been shown to outperform two existing methods. The obstacle avoidance scheme has been established using potential functions, in order to be used for either enabling any robot to independently avoid any obstacle or moving all the robots to keep in formation at any time. The performance and merit of the proposed control and obstacle avoidance method has been shown effective through simulations on the multiple IASBRRs. Future work will be conducting more formation experiments with three IASBSSs to show applicability of the proposed method.

## Acknowledgements

The authors deeply acknowledge financial support from Ministry of Science and Technology (MOST), Taiwan, ROC, under contract MOST 108-2638-E-005-001-MY2.

## References

[1] R. Olfati-Saber and R. Murray, “Distributed cooperative control of multiple vehicle formations using structural potential functions,” *IFAC World Congress*, Barcelona, Spain, July 2002.

[2] W. Kang, N. Xi, and A. Sparks, “Formation control of autonomous agents in 3D workspace, ” in *Proc. of 2000 IEEE International Conference on Robotics and Automation*, San Francisco, CA, 2000.

[3] P. Ogren and N. E. Leonard, "Obstacle avoidance in formation," 2003 IEEE International Conference on Robotics and Automation, Taipei, Taiwan, pp. 2492-2497 vol.2, 2003.

[4] C. L. P. Chen, Z. L. Liu, and S. Feng, “A new paradigmatic broad learning system: Structural variations and universal approximation capability,” *IEEE Trans. Neural Netw. Learn. Syst., vol. 30, no. 4, pp. 1191-1204, Apr. 2019.*

[5] C. L. P. Chen and Z. L. Liu, “Broad learning system: an effective and efficient incremental learning system without the need for deep architecture,” IEEE Trans. Neural Netw. Learn. Syst., vol. 29, no. 1, pp. 10-24, Jan. 2018.

[6] M. L. Xu, M. Han, C. L. P. Chen, and T. Qiu, “Recurrent broad learning systems for time series prediction,” *IEEE Trans. Cybern.*,vol 50, no.4, pp. 1405-1417, April 2020.

[7] R. Hollis, “Ballbots,” *Scientific American Mag.*, pp. 72-77, Oct. 2006.

[8] C. C. Tsai, C. K. Chan, and L. C. Kuo, “LQR Motion Control of a Ball-Riding Robot,” *Proc. of 2012 IEEE Intern.Conf. on Advanced Intelligent Mechatronics*, Kaohsiung, Taiwan, July 11-14, 2012.

[9] Single-Wheeled Mobile Robot with Inverse Mouse-Ball Drive,” *Proc. of the IEEE Intern. Conf. on Robotics and Automation*, Orlando, USA, pp. 2884-2889, 2006.

[10] U. Nagarajan, A. Mampetta, G. A. Kantor, and R. L. Hollis, “State transition, balancing, station keeping, and yaw control for a dynamically stable single spherical wheel mobile robot” in *Proc.IEEE Int. Conf. Robot. and Autom.*, pp. 998-1003.,2009.

[11] U. Nagarajan, G. A. Kantor, and R. L. Hollis, “Trajectory planning and control of an underactuated dynamically stable single spherical wheeled mobile robot” in *Proc. IEEE Int. Conf. Robot. And Autom.*, pp. 3743-3748, 2009.

[12] M. Kumagai and T. Ochiai, “Development of a Robot Balancing on a Ball” in *Proc. IEEE Int. Conf. Contr. Autom. And Systems*, pp. 433-438, 2008.

[13] M. Kumagai and T. Ochiai, “Development of a Robot Balancing on a Ball- Application of passive motion transportation,” in *Proc. IEEE Int. Conf. Robot. And Autom.*, pp. 4106-4111, 2009.

[14] C. Tsai, Y. Ciou, F. Tai, S. Su, and C. Lin, "Backstepping station-keeping control using recurrent wavelet fuzzy CMAC for ball-driven chairs," in *Proc. 2014 Inter.Conf. on Machine Learning and Cybernetics*, Lanzhou, 2014, pp. 721-727.

[15] F. C. Tai, *Intelligent Adaptive Distributed Consensus Formation Control of Networked Multiple Ball-Riding Robots*, Master Thesis, E E Department, National Chung Hsing University, January 2018.

[16] S. T. Chen, *Collison-free sliding-mode trajectory tracking and cooperative formation control using output recurrent broad learning system and artificial potential function for gyro-stabilized ball-riding robots*, Master Thesis, EE Department NCHU, July 2020.

[17] C. K. Chan and C. C. Tsai, "Intelligent backstepping sliding-mode control using recurrent interval type 2 fuzzy neural networks for a ball-riding robot," *2012 Intern. Conf. on Fuzzy Theory and Its Applications (iFUZZY2012)*, Taichung, 2012, pp. 169-174.

[18] B. Y. Chen, *Trajectory tracking and cooperative formation control using broad learning system and sliding-mode control for gyro-stabilized ball-riding robots*, Master Thesis, EE Department, NCHU, July 2019.